ORIGINAL PAPER

Analysis of coronary arterial calcification components with coronary CT angiography using single-source dual-energy CT with fast tube voltage switching

Kazuhiro Matsui · Haruhiko Machida · Tetsuya Mitsuhashi · Hisako Omori · Takashi Nakaoka · Hiroshi Sakura · Eiko Ueno

Abstract Clinical cardiac applications of single-source dual-energy computed tomography (DECT) have recently been introduced. This study aimed to analyze the components of coronary arterial calcification (CAC) in vivo by material decomposition achieved with DECT. We reconstructed computed tomography (CT) angiography images for 51 consecutive patients with CACs who had undergone electrocardiography-gated coronary CT angiography by single-source DECT with fast tube voltage switching. We placed regions of interest (ROIs) within the CAC with margins of at least 0.5 mm to minimize partial volume averaging. We compared histograms for the effective atomic number (EAN) and the median, mean, and maximum EANs for each CAC with the theoretical EANs for possible CAC components, including hydroxyapatite (HA), calcium oxalate monohydrate (COM), and dicalcium phosphate dehydrate. We also investigated the in vivo EAN for COM and in vitro EAN for HA by our phantom experiment. Analysis of the CAC components was feasible in 177 ROIs from 28 patients. The median EAN was 13.8 ± 0.8 (95 % con-fidence interval 13.7–13.9), which is similar to the theoretical EAN for COM (13.8). The EAN for HA in vitro was 16.5 ± 0.1, which was slightly higher than the theoretical EAN value for HA (16.1). Notably, the median EAN in 144 ROIs (81.4 %) was between 11.2 and 14.4, which is the reported range of the in vivo EAN for COM. Our results suggest that COM might be a more frequent CAC component than previously reported.

Keywords Coronary artery calcification · Coronary computed tomography · Calcium oxalate monohydrate · Dual-energy computed tomography · Effective atomic number

Abbreviations

ASiR	Adaptive statistical iterative reconstruction
CABG	Coronary artery bypass graft
CAC	Coronary arterial calcification
CAD	Coronary artery disease
CC	Calcium carbonate
CI	Confidence interval
CO	Calcium oxalate
COM	Calcium oxalate monohydrate
CT	Computed tomography
CTA	Computed tomography angiography
CTDIvol	Volume CT dose index
DCPD	Dicalcium phosphate dehydrate
DECT	Dual-energy computed tomography
DLP	Dose-length product
EAN	Effective atomic number
ECG	Electrocardiogram
HA	Hydroxyapatite
OCP	Octacalcium phosphate
ROI	Region of interest

K. Matsui · T. Mitsuhashi · H. Omori · T. Nakaoka (✉) ·
H. Sakura
Departments of Medicine, Tokyo Women's Medical University
Medical Center East, 2-1-10 Nishiogu, Arakawa-ku,
Tokyo 116-8567, Japan
e-mail: nakaokgm@dnh.twmu.ac.jp

H. Machida (✉) · E. Ueno
Departments of Radiology, Tokyo Women's Medical University
Medical Center East, 2-1-10 Nishiogu, Arakawa-ku,
Tokyo 116-8567, Japan
e-mail: machira@dnh.twmu.ac.jp

Introduction

Coronary arterial calcification (CAC) is a prominent feature of an advanced form of atherosclerosis. CAC correlates most strongly with the incidence of cardiovascular diseases, and is associated with the poorest prognosis in patients with coronary artery disease (CAD) compared with other risk markers, such as high-sensitivity C-reactive protein [1, 2]. However, the biological significance of CAC in the atherosclerotic process and its influence on the prognoses of atherosclerotic patients remain contentious.

Calcium deposits in cardiovascular tissues are composed of calcium carbonate (CC), calcium oxalate (CO), hydroxyapatite (HA), dicalcium phosphate dehydrate (DCPD), and octacalcium phosphate (OCP) [3, 4]. HA is not only the major component of bone, but is also the predominant component of arterial calcification, accounting for more than 70 %, followed by CC [5].

The use of coronary computed tomography (CT) angiography (CTA) has greatly expanded because it is a powerful tool for the noninvasive diagnosis of CAD, including myocardial infarction and angina pectoris. Additionally, CTA is useful in postoperative follow-up of patients undergoing percutaneous coronary intervention or coronary artery bypass graft (CABG) surgery. However, in current coronary CTA studies, the presence of CAC hinders accurate evaluation of coronary artery stenosis.

Recently, clinical cardiac applications of single-source dual-energy CT (DECT) have been introduced. This CT technology is capable of simultaneously acquiring both high—(140 kVp) and low-energy (80 kVp) datasets. DECT can perform material decomposition by material density imaging when two different materials, such as iodine and water, are selected as the basis pair. Effective atomic number (EAN), which is a descriptor of the density and the atomic number of a material, can also be derived from DECT datasets and used to differentiate materials [6]. These DECT-based material decomposition and differentiation techniques have been reported to accurately reveal components of urinary stones by EAN [7]. Therefore, EAN is also expected to provide clinically useful information on CAC components. Furthermore, EAN-based evaluation might allow accurate evaluation of coronary artery stenosis, even in the presence of CAC, when iodine and the CAC component are selected as the basis pair for coronary CTA.

Therefore, the purpose of the present study was to perform an in vivo analysis of CAC components based on EAN in coronary CTA studies using DECT.

Methods

Study population

We retrospectively searched the electronic database at our radiology department for patients who had undergone electrocardiography (ECG)-gated cardiac DECT between June 2012 and March 2013 with a single-source DECT scanner (Discovery CT750 HD; GE Healthcare, Milwaukee, WI) with fast tube voltage switching from 80 to 140 kVp during a single projection in 0.25 ms. Exclusion criteria included insufficient breath hold. Fifty-five consecutive patients underwent ECG-gated contrast-enhanced cardiac DECT with fast tube voltage switching. However, we could not identify CAC in 4 of the 55 patients in a low-dose axial scan. Therefore, the remaining 51 patients were enrolled in the present study.

Fast tube voltage switching for cardiac CT was performed with a prospective ECG-gated step-and-shoot axial scan technique (Snap-Shot Pulse; GE Healthcare). At our institution, this technique is used in patients with a mean heart rate of less than 65 beats per minute (bpm) and heart rate variability (defined as the standard deviation of the heart rate) of <5 bpm. Unless contraindicated, patients with heart rates higher than 60 bpm were orally administered metoprolol (1 mg/kg of body weight; Seloken; Astra Zeneca, Tokyo, Japan) 90 min before each CTA examination to lower heart rate. This study was approved by the Institutional Review Board of Tokyo Women's Medical University.

CT scanning technique

The scan sequence included a scout scanogram, a low-dose axial scan, a test bolus scan, and a clinical cardiac scan. We only performed a DECT scan for the clinical cardiac scan and performed a standard single-energy CT scan for other scans. All of the patients were administered 0.3 mg of nitroglycerin (Nitropen; Nippon Kayaku, Tokyo, Japan) sublingually immediately before acquisition of the localization images. We performed low-dose axial scans to determine the calcium score and the coverage range (approximately 16 cm for patients who had not undergone CABG surgery) for the clinical cardiac scan, which includes the entire heart.

The test bolus was tracked in the ascending aorta at the level of the pulmonary trunk every 2 s after intravenous administration of 10 mL of iomeprol (Iomeron; Eisai, Tokyo, Japan) with an iodine concentration of 350 mg/mL. This was followed by a 15-mL saline bolus injection at the same rate as the test bolus into an antecubital vein via a 20-gauge catheter using an automatic double-head power injector (Dual Shot GXV; Nemoto-Kyorindo, Tokyo,

Japan). We then performed a cardiac scan with a delay after administration of the contrast medium that was calculated during the test bolus scan. A bolus of contrast medium at a rate of 25 mg/kg body weight per second was injected for 14 s. This was followed by a bolus injection of 30 mL of saline at the same rate using the injector. We performed the cardiac scan during a single breath hold in the head-to-foot direction using the following scan parameters: tube current, 600 mA; rotation time, 350 ms; temporal resolution, 175 ms; collimation, 64×0.625 mm; and padding time, 80–120 ms.

We recorded the volume CT dose index (CTDIvol, measured in mGy) and dose-length product (DLP, measured in mGy × cm) that were displayed on the dose report on the CT scanner for each CT scan. We calculated the mean CTDIvol and DLP in all the patients. We approximated the mean effective dose (ED) in the patients using the following equation: ED = κ × DLP, where κ is equal to 0.014 mSv × mGy^{-1} × cm^{-1}. This value is applicable for chest CT examinations for adult individuals [8].

Post-processing of images

From the data acquired during the CT scanning, we reconstructed monochromatic axial images at 65 keV, with a slice thickness of 0.625 mm and a field of view of 5×5 cm^2 in the best cardiac phase during the diastolic phase. We used the standard kernel and adaptive statistical iterative reconstruction (ASiR) with a blending ratio of 50 % with a filtered back-projection algorithm [9]. We transferred the reformatted images to an external dedicated workstation (Advantage Workstation version 4.5; GE Healthcare) for post-processing, which is described below.

Using the dedicated software for DECT analysis (GSI Viewer; GE Healthcare) that was installed in the workstation, two experienced observers of coronary CTA placed a circular region of interest (ROI) with an area of 0.5×0.5 cm^2 with margins of 0.5 mm or more within each CAC in consensus. They simultaneously subjectively assessed the susceptibility of each CAC to errors from partial volume averaging by noncalcified structures on the contiguous slices used for CAC component analysis by EAN. CACs that were considered sufficiently susceptible to such errors were excluded from the subsequent analysis. When CAC on a certain axial image was sufficiently extensive for multiple ROI placements, the observers placed the first ROI with a margin of 0.5 mm or more from the most proximal end. They then placed the second ROI 1 cm or more distal from the first ROI. The ROIs continued to be placed in this manner. Finally, the last ROI was placed with a margin of 0.5 mm or more from the most distal end of the CAC.

For each ROI placed within the CAC, we obtained the following: (1) a histogram of the EAN that represented the EAN value on the x-axis and the ratio of the number of the pixels showing the corresponding EAN value to the number of all pixels within the ROI on the y-axis; and (2) the EAN value of each pixel included, to calculate the median, mean, and maximum EAN values for all of the pixels that were included. If the histogram for a certain CAC showed a dull (i.e., broad and low) peak (i.e., the distribution of EAN was greatly scattered), possibly attributable to errors arising from partial volume averaging, this CAC was also excluded from the subsequent analysis.

Evaluation of EAN

For each ROI within the CAC, we semi-quantitatively compared the EAN value that showed a peak in the histograms, defined as "the peak EAN", with the theoretical EAN values for HA (16.1), calcium oxalate monohydrate (COM; 13.8), DCPD (11.2), and OCP (10.0). These theoretical values were obtained from the website of the National Institute of Standards and Technology (NIST) (http://physics.nist.gov/PhysRefData/Xcom/html/xcom1.html) and introduced into GSI Viewer.

We used a cylindrical cardiac phantom (ALPHA 1-VTPC; Fuyo Corporation, Tokyo, Japan) that was filled with iodine contrast medium, iomeprol, with an iodine concentration of 350 mg/mL diluted to show 350 HU at 120 kVp. A dense square-shaped HA pellet ($10 \times 10 \times 2$ mm^3) that had a purity of 98 % or greater and a relative density of 99 % or greater (APP-100; HOYA Technosurgical, Tokyo, Japan) was attached on the surface of the phantom. The pellet was entirely submerged in degassed water that filled an acryl tank and was placed on a CT scanner bed with the long axis of the phantom parallel to the z axis. The reference EAN for HA was determined in vitro by scanning the HA pellet using the same DECT technique and scan parameters as mentioned above with a padding time of 80 ms. We also quantitatively compared the median, mean, and maximum EAN values with the EAN values for pure COM that were reported in a previous study that used a similar in vivo DECT technique [7].

Statistical analysis

Statistical analysis was performed using StatView for Windows (version 5.0; SAS Institute, Cary, NC). A *P* value of less than 0.05 was considered statistically significant.

Table 1 Patients' characteristics

	All patients		EAN analyzed patients	
Gender (M/F)	31/20	N = 51	20/8	N = 28
Age (years)	69.5 ± 9.4	N = 51	71.4 ± 8.1	N = 28
Bodyweight (kg)	61.7 ± 11.7	N = 48	64.4 ± 11.2	N = 27
SBP (mmHg)	135 ± 15	N = 46	137 ± 12	N = 26
DBP (mmHg)	82 ± 12	N = 46	81 ± 12	N = 26
Serum creatinine (mg/dl)[a]	0.8 ± 0.2	N = 45	0.8 ± 0.2	N = 25
Previous MI	3	N = 50	3	N = 28
Recent angina pectoris	13	N = 50	8	N = 28
PCI	3	N = 50	2	N = 28
CABG	7	N = 50	7	N = 28
Congestive heart failure	0	N = 50	0	N = 28
HbA1c (%)	5.8 ± 0.8	N = 38	5.8 ± 0.8	N = 23
Diabetes mellitus	9	N = 49	5	N = 28
Hypertension	33	N = 49	21	N = 28
Hemodialysis	3	N = 51	3	N = 28

CABG coronary artery bypass graft, *DBP* diastolic blood pressure, *MI* myocardial infarction, *N* number of patients whose data were available, *PCI* percutaneous coronary intervention, *SBP* systolic blood pressure

[a] Hemodialysis patients were excluded. Data are means ± standard deviations (SD) or numbers of patients

Results

Patients' characteristics

The patients consisted of 31 men and 20 women. Myocardial infarction was diagnosed in three patients and recent angina pectoris in 13 patients. Percutaneous coronary intervention was performed in three patients and CABG surgery in seven patients (Table 1). CACs that were considered sufficiently susceptible to errors from partial volume averaging were excluded from the subsequent analysis. As a result, a total of 177 ROIs from 28 patients were available for subsequent CAC component analysis.

Phantom analysis

We determined the EAN for HA in vitro by placing a total of nine ROIs (2 × 2 mm^2) on three different slices of the HA pellet. The EAN for HA in vitro was 16.5 ± 0.1 (range 16.1–16.6), which is slightly higher than the theoretical EAN value of HA (16.1) (Fig. 1).

Radiation doses

The mean CTDIvol and DLP values of low-dose axial scans, test bolus scans, and clinical cardiac scans are shown in Table 2. The mean total effective dose from the low-
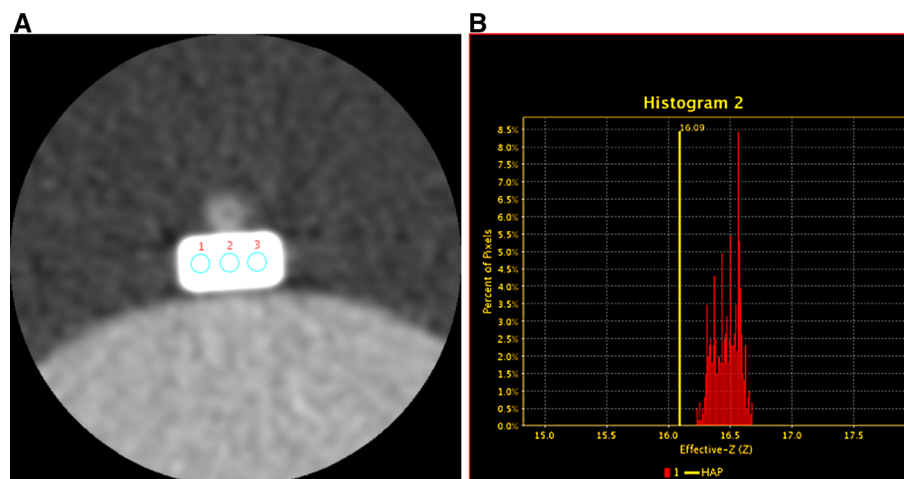
Fig. 1 Determination of effective atomic number (EAN) for hydroxyapatite (HA) in vitro. **a** An axial monochromatic image at 65 keV of a dense square-shaped HA pellet (10 × 10 × 2 mm^2). The pellet is attached on the surface of a cylindrical cardiac phantom that is filled with iodine contrast medium and entirely submerged in degassed water. Three circular regions of interest (2 × 2 mm^2) were placed within the HA pellet with no overlap in a single slice. **b** Representative histogram of the EAN for an HA pellet (*red bars*) with the theoretical EAN value for HA (*orange line*)

Table 2 Mean radiation dose

	All patients (n = 51)	Patients without CABG (n = 44)	Patients with CABG (n = 7)
Low dose CTDIvol (mGy)	12.3 ± 3.4	12.1 ± 3.6	13.5 ± 2.4
Low dose DLP (mGy × cm)	200.3 ± 77.2	183.9 ± 55.8	303.4 ± 113.9
Bolus CTDIvol (mGy)	61.9 ± 15.0	61.3 ± 15.3	65.8 ± 13.1
Bolus DLP (mGy × cm)	31.0 ± 7.5	30.7 ± 7.7	32.9 ± 6.5
Clinical CTDIvol (mGy)	21.7 ± 2.8	21.4 ± 2.6	23.6 ± 3.4
Clinical DLP (mGy × cm)	316.6 ± 100.3	289.6 ± 47.0	486.1 ± 171.0
Total DLP (mGy × cm)	547.9 ± 162.8	504.2 ± 75.8	822.3 ± 279.1

The volume CT dose index (CTDIvol) and dose length product (DLP) of a low-dose axial scan (Low dose), a test bolus scan (Bolus), and a clinical cardiac scan (Clinical) and the sum of the DLP of these three scans (Total) were shown. *CABG* coronary artery bypass graft

dose axial scan, test bolus scan, and clinical cardiac scan was 7.7 ± 2.3 mSv. The mean effective dose of the clinical cardiac scan of patients with CABG surgery was 6.8 ± 2.4 mSv, which was significantly higher than that without CABG surgery (4.1 ± 0.7 mSv, $P = 0.02$), because the coverage range included graft vessels in addition to the entire heart.
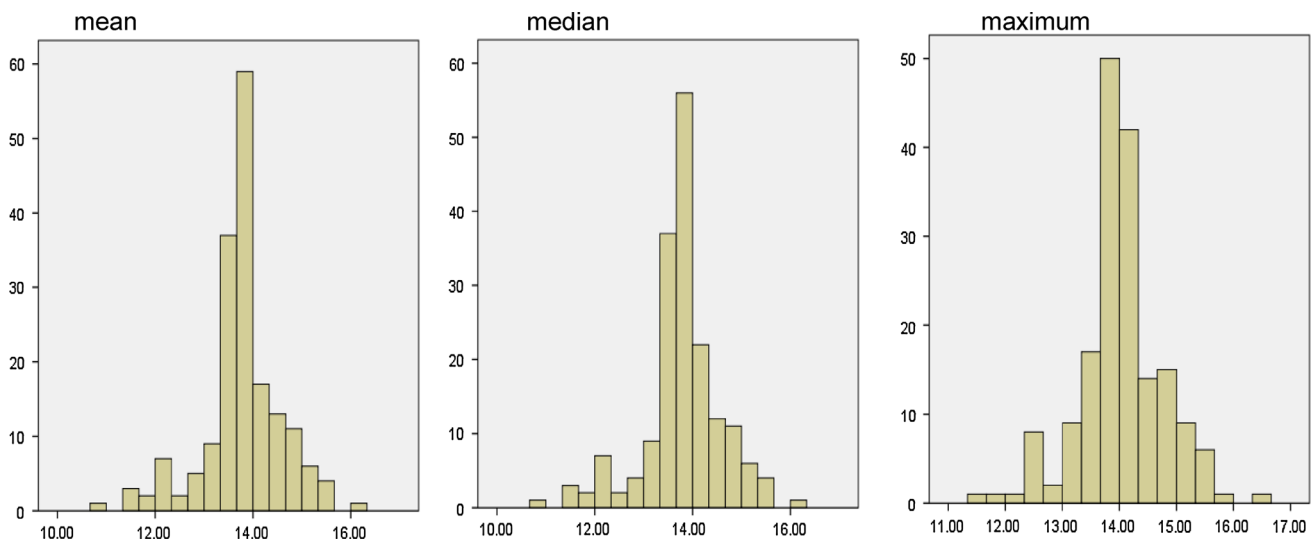
EAN values for CAC

In 175 ROIs (98.8 %) within the CACs, the peak EAN was localized between the theoretical EAN for HA (16.1) and that for DCPD (11.2). The median EAN value for all of the ROIs placed within CACs was 13.8 ± 0.8 (95 % confidence interval [CI] 13.7–13.9), which is similar to the theoretical EAN for COM (13.8). The mean and maximal EAN values were 13.8 ± 0.8 (95 % CI 13.7–13.9) and 14.0 ± 0.7 (95 % CI 13.9–14.1), respectively (Fig. 2).

The median EAN value for 144 ROIs (81.4 %) ranged between 11.2 and 14.4. The mean and maximum EAN values were between 11.2 and 14.4 in 143 ROIs (80.8 %) and 139 ROIs (78.5 %), respectively. The median EAN value was <11.2 in one ROI (0.6 %) and greater than 14.4 in 32 ROIs (18.1 %).

Histogram analysis

Some of the EAN peaks were almost identical to those of HA, COM, and DCPD. Specifically, in a 65-year-old man, the peak EAN for an ROI within CAC in segment 6 (according to the American Heart Association classification) of the left anterior descending artery was similar to the theoretical EAN for HA (16.1) (Fig. 3a). In the same patient, the peak EAN for an ROI within another CAC in segment 1 of the right coronary artery was identical to the EAN for COM (13.8) (Fig. 3b). In a 71-year-old man, the peak EAN for a ROI within CAC in segment 5 of the left

Fig. 2 Mean, median, and maximal EAN values for 177 ROIs. *EAN* effective atomic number, *ROI* region of interest

Fig. 3 Analysis of various CAC components using EAN histograms (*left*, a CPR monochromatic image of coronary CTA at 65 keV; *right*, an EAN histogram for each CAC). The *light brown*, *blue*, *green*, and *red lines* in the histograms (*right*) represent the EANs of hydroxyapatite (HA; 16.1), calcium oxalate monohydrate (COM; 13.8), dicalcium phosphate dehydrate (DCPD; 11.2), and octacalcium phosphate (OCP; 10.0), respectively. **a** CTA of a 65-year-old man where a circular ROI was placed within a CAC (*arrow*) in segment 6 of the left anterior descending artery (*left*). The *yellow* histogram obtained from the ROI is located near the EAN for HA (16.1), represented by the *light brown line* (*right*). **b** CTA of a 65-year-old man (the same patient as shown in **a**) where a circular ROI was placed within a CAC (*arrow*) in segment 1 of the right coronary artery (*left*). The *yellow* histogram obtained from the ROI is located at the EAN for COM (13.8), represented by the *blue line* (*right*). **c** CTA of a 71-year-old man. A circular ROI was placed within a CAC (*arrow*) in segment 5 of the left coronary artery (*left*). The *yellow* histogram obtained from the ROI is located near the EAN for DCPD (11.2), represented by the *green line* (*right*). CAC, coronary arterial calcification, *CPR* curved multiplanar reformation, *CTA* computed tomography angiography, *EAN* effective atomic number
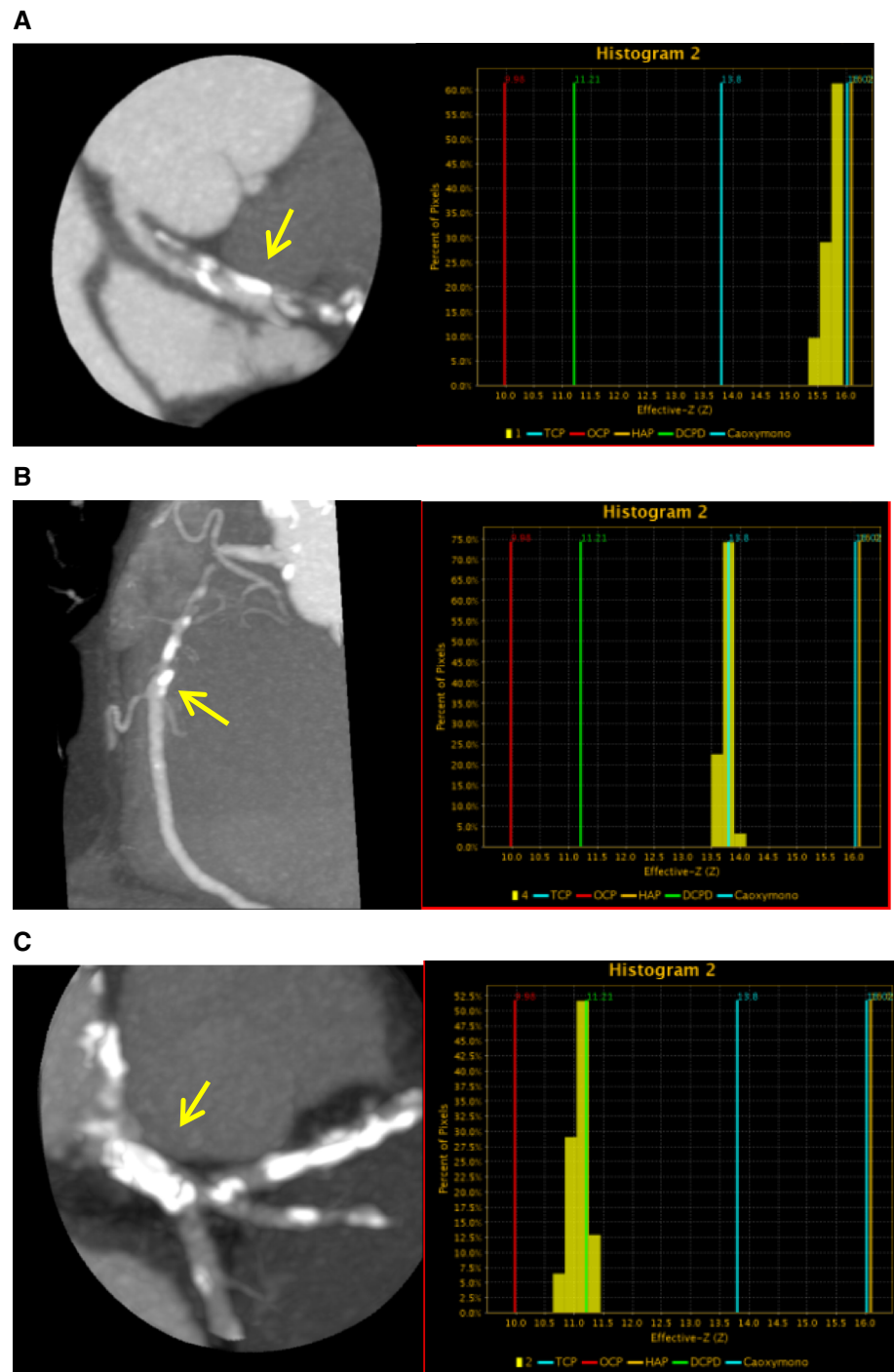
main coronary artery was similar to the EAN for DCPD (11.2) (Fig. 3c).

Figure 4 shows the EANs within four different CACs in segments 1–3 of the right coronary artery in a 70-year-old man with unstable angina. The peak EAN for one ROI was similar to the theoretical EAN for COM (13.8) (Fig. 4a). In contrast, the peak EAN for the other three ROIs was between the EANs for DCPD and COM (Fig. 4b–d).

Different CACs showed various compositions, even in the same patient.

Discussion

Historically, the composition of calcified plaques in arteries has been analyzed by ashing the samples obtained from the

Fig. 4 Analysis of components of four different CACs in a 70-year-old man with unstable angina using EAN histograms. **a** A CPR monochromatic image of coronary CTA of the right coronary artery at 65 keV. **b–e** Four ROIs were placed within CACs in segments 1–3. *Yellow* (**b**), *red* (**c**), *pink* (**d**), and *blue* (**e**) histograms were obtained from CACs and are labeled as B–E, respectively. The *light brown*, *blue*, *green*, and *red lines* in the histograms (*right*) represent the EANs for hydroxyapatite (HA; 16.1), calcium oxalate monohydrate (COM; 13.8), dicalcium phosphate dehydrate (DCPD; 11.2), and octacalcium phosphate (OCP; 10.0), respectively. *CAC* coronary arterial calcification, *CPR* curved multiplanar reformation, *CTA* computed tomography angiography, *EAN* effective atomic number
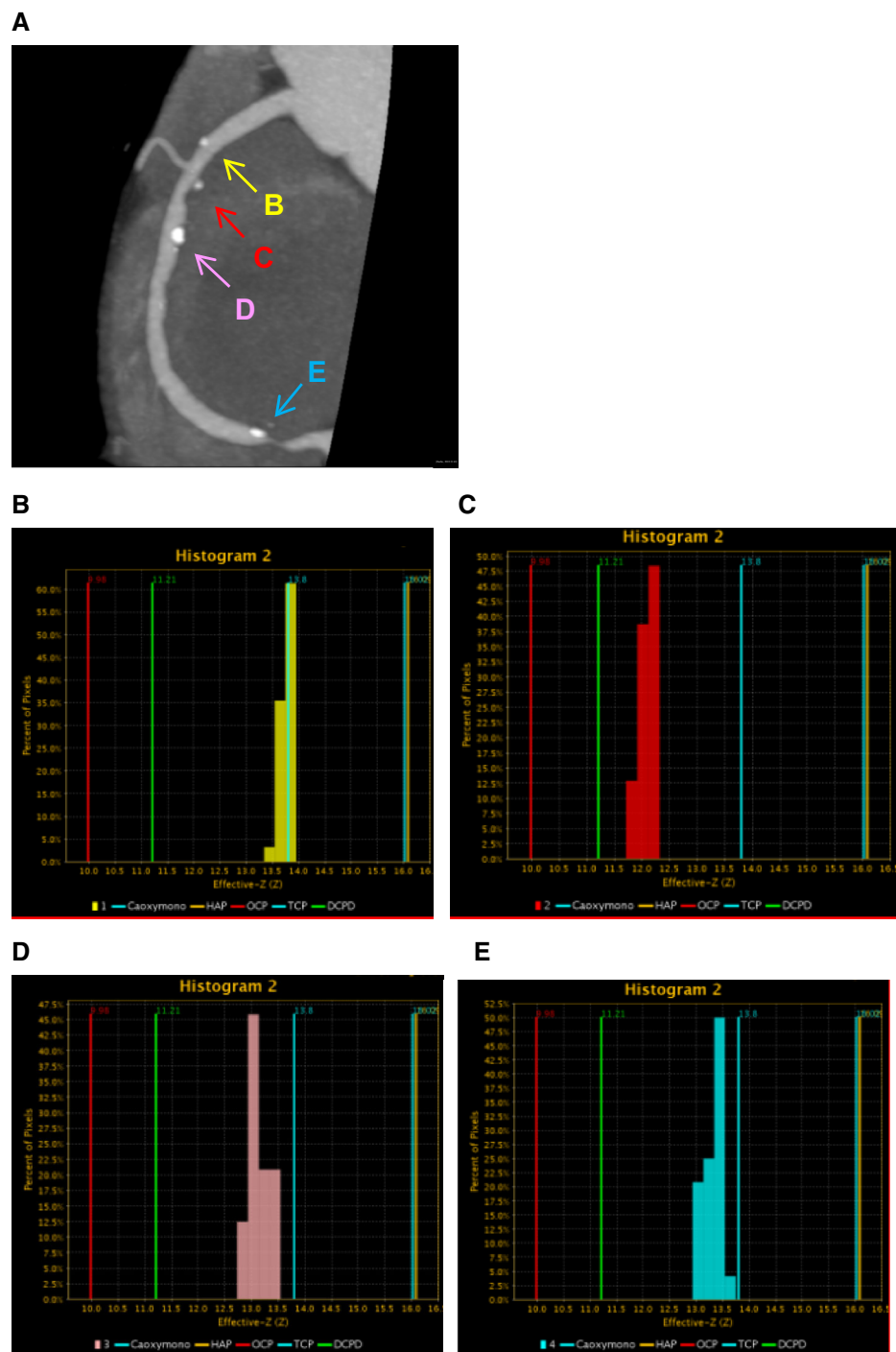
thoracic or abdominal aorta during autopsy or carotid endarterectomy. Mineral deposits obtained from the human atherosclerotic thoracic or abdominal aorta have been treated with acid and analyzed [5]. However, even with such chemical analyses, discrimination of Ca $(COO)_2$ (i.e., CO) and $CaCO_3$ (i.e., CC) can be difficult because CO and CC dissolve equally well during treatment with hydrochloric acid.

In the early twentieth century, calcification of the medial layer of the arteries was reported to result from Mönckeberg-type sclerosis [10]. However, bone marker proteins, including bone morphogenetic proteins [11], osteopontin [12], bone sialoprotein, and matrix Gla protein, are abundantly expressed in atherosclerotic lesions [13]. This suggests that arterial calcification is regulated through a mechanism similar to that involved in bone formation.

There is also an untested hypothesis that CAC strengthens atherosclerotic plaques that are vulnerable to rupture [14].

In a recent study [7], the use of EAN allowed accurate substratification of renal stone components into uric acid, struvite, and COM in vivo with single-source DECT. Notably, the EANs of pure COM determined in vivo and in vitro are closely related (EAN range in vivo: 11.2–14.4; EAN range in vitro: 12.1–13.8). The EAN of most of the CACs in our study corresponded to the range for pure COM determined in vivo in a previous study rather than the theoretical EAN for HA (16.1) or EAN for HA determined in vitro (16.5 ± 0.1) [7].

Although few studies have referred to the chemical composition of CAC, calcified plaques of the coronary artery have been reported to contain HA, by using energy-dispersive x-ray microanalysis [12] or molecular imaging probes [4]. We are unsure why the EAN of a relatively small number of CACs corresponded with the EAN for HA in vivo. A certain percentage of HA might be present as a carbonate complex [5]. HA has the highest EAN among the possible components of CAC mentioned above. Therefore, the EAN of CACs can be lower than that of HA, depending on the percentage of HA present, even in CACs mainly composed of HA. CO crystals have also been detected in coronary atherosclerotic plaques of four patients, including three with acquired immunodeficiency syndrome [15]. Additionally, CO deposition in large vessels, such as the abdominal aorta, has been recognized since the 1970s [16]. Notably, EAN is not supposed to be dependent on the density of materials [6].

The protocol of DECT with fast tube voltage switching that was used in our study is consistent with a previous study that showed significant noise reduction and an improvement in image quality with optimal combinations of energy levels (65–75 keV) and ASiR blending ratios (40–60 %) in monochromatic imaging of coronary CTA [9]. Standard retrospective ECG-gated helical scanning with a low helical pitch yields a higher effective dose [17]. A recent systematic review reported that the mean effective dose of prospective ECG-gated scans (4.5 mSv) was significantly lower than that of retrospective scans (13.8 mSv) [18]. The radiation dose of clinical cardiac scans in our study (i.e., 4.3 mSv) was within the range of radiation dose of the prospective ECG-gated scan. The radiation dose of the clinical cardiac scan of patients with CABG surgery was also lower than that of retrospective scans [19]. The reconstructed field of view (5×5 cm^2) that was used in this study is the smallest available with the CT scanner that we used. However, this spatial resolution (pixel size of approximately 0.1×0.1 mm^2) is still inferior to that achieved with other imaging modalities with excellent spatial resolution, including intravascular ultrasound and optical coherence tomography. Accurate analysis of CAC composition is also

expected to shed light on how CAC composition affects the rupture of coronary arterial plaques in the future.

Study limitations

Our study was limited by several factors. First, this was a retrospective study and included a relatively small study population. A large-scale prospective study may be warranted to confirm our results. Second, only EAN values in vivo and in vitro for COM and EAN values in vitro for HA were available as a reference, whereas EAN values for the other CAC components, such as CC and DCPD, were not available. Therefore, our analysis of CAC components may have been limited, particularly with respect to CC and DCPD. Third, because EAN values are supposed to vary depending on the heterogeneity of the material [20], the EAN value itself is not able to pinpoint the component. Finally, although radiation doses of a scout scanogram are supposed to be small, they should also be considered in the overall evaluation.

Conclusions

We performed in vivo analysis of CAC components using EANs obtained with coronary CTA using single-source DECT with fast tube voltage switching. Our results suggest that COM could be a more frequent CAC component than previously reported, together with HA and CC.

References

1. Yeboah J, McClelland RL, Polonsky TS, Burke GL, Sibley CT, O'Leary D, Carr JJ, Goff DC, Greenland P, Herrington DM (2012) Comparison of novel risk markers for improvement in cardiovascular risk assessment in intermediate-risk individuals. JAMA 308(8):788–795. doi:10.1001/jama.2012.9624
2. Margolis JR, Chen JT, Kong Y, Peter RH, Behar VS, Kisslo JA (1980) The diagnostic and prognostic significance of coronary artery calcification. A report of 800 cases. Radiology 137(3): 609–616
3. Carlstrom D, Engfeldt B, Engstrom A, Ringertz N (1953) Studies on the chemical composition of normal and abnormal blood vessel walls. I. Chemical nature of vascular calcified deposits. Lab Invest 2(5):325–335
4. Lee JS, Morrisett JD, Tung CH (2012) Detection of hydroxyapatite in calcified cardiovascular tissues. Atherosclerosis 224(2): 340–347. doi:10.1016/j.atherosclerosis.2012.07.023

5. Schmid K, McSharry WO, Pameijer CH, Binette JP (1980) Chemical and physicochemical studies on the mineral deposits of the human atherosclerotic aorta. Atherosclerosis 37(2):199–210

6. Spiers FW (1946) Effective atomic number and energy absorption in tissues. Br J Radiol 19:52–63

7. Kulkarni NM, Eisner BH, Pinho DF, Joshi MC, Kambadakone AR, Sahani DV (2013) Determination of renal stone composition in phantom and patients using single-source dual-energy computed tomography. J Comput Assist Tomogr 37(1):37–45. doi:10.1097/RCT.0b013e3182720f66

8. Valentin J (2007) Managing patient dose in multi-detector computed tomography(MDCT). ICRP Publication 102. Annals of the ICRP 37(1):1–79, iii

9. Fuchs TA, Stehli J, Fiechter M, Dougoud S, Gebhard C, Ghadri JR, Husmann L, Gaemperli O, Kaufmann PA (2013) First experience with monochromatic coronary computed tomography angiography from a 64-slice CT scanner with Gemstone Spectral Imaging (GSI). J Cardiovasc Comput Tomogr 7(1):25–31. doi:10.1016/j.jcct.2013.01.004

10. Micheletti RG, Fishbein GA, Currier JS, Fishbein MC (2008) Monckeberg sclerosis revisited: a clarification of the histologic definition of Monckeberg sclerosis. Arch Pathol Lab Med 132(1):43–47. doi:10.1043/1543-2165(2008)132[43:MSRACO]2.0.CO;2

11. Bostrom K, Watson KE, Horn S, Wortham C, Herman IM, Demer LL (1993) Bone morphogenetic protein expression in human atherosclerotic lesions. J Clin Invest 91(4):1800–1809. doi:10.1172/JCI116391

12. Fitzpatrick LA, Severson A, Edwards WD, Ingram RT (1994) Diffuse calcification in human coronary arteries. Association of osteopontin with atherosclerosis. J Clin Invest 94(4):1597–1604. doi:10.1172/JCI117501

13. Giachelli CM, Bae N, Almeida M, Denhardt DT, Alpers CE, Schwartz SM (1993) Osteopontin is elevated during neointima formation in rat arteries and is a novel component of human atherosclerotic plaques. J Clin Invest 92(4):1686–1696. doi:10.1172/JCI116755

14. Doherty TM, Detrano RC (1994) Coronary arterial calcification as an active process: a new perspective on an old problem. Calcif Tissue Int 54(3):224–230

15. Fishbein GA, Micheletti RG, Currier JS, Singer E, Fishbein MC (2008) Atherosclerotic oxalosis in coronary arteries. Cardiovasc Pathol 17(2):117–123. doi:10.1016/j.carpath.2007.07.002

16. Arbus GS, Sniderman S (1974) Oxalosis with peripheral gangrene. Arch Pathol 97(2):107–110

17. Schroeder S, Achenbach S, Bengel F, Burgstahler C, Cademartiri F, de Feyter P, George R, Kaufmann P, Kopp AF, Knuuti J, Ropers D, Schuijf J, Tops LF, Bax JJ (2008) Cardiac computed tomography: indications, applications, limitations, and training requirements: report of a Writing Group deployed by the Working Group Nuclear Cardiology and Cardiac CT of the European Society of Cardiology and the European Council of Nuclear Cardiol. Eur Heart J 29(4):531–556. doi:10.1093/eurheartj/ehm544

18. Sun Z, Ng KH (2012) Prospective versus retrospective ECG-gated multislice CT coronary angiography: a systematic review of radiation dose and diagnostic accuracy. Eur J Radiol 81(2):e94–100. doi:10.1016/j.ejrad.2011.01.070

19. Machida H, Masukawa A, Tanaka I, Fukui R, Suzuki K, Ueno E, Kodera K, Nakano K, Shen Y (2010) Prospective electrocardiogram-gated axial 64-detector computed tomographic angiography vs retrospective gated helical technique to assess coronary artery bypass graft anastomosis: comparison of image quality and patient radiation dose. Circ J 74(4):735–740

20. Murty RC (1965) Effective atomic numbers of heterogeneous materials. Nature 207:398–399